

# Electron density variations during ultraviolet transient events

L. Teriaca<sup>†</sup> (lte@arcetri.astro.it), M. S. Madjarska  
(madj@star.arm.ac.uk) and J. G. Doyle (jgd@star.arm.ac.uk)  
*Armagh Observatory, College Hill, Armagh BT61 9DG, N. Ireland*

**Abstract.** High-resolution temporal observations performed with the SUMER spectrometer on SoHO provide an opportunity to investigate the electron density variations in the ‘quiet Sun’ solar transition region due to UV transient events. Two datasets obtained in the density sensitive lines belonging to the O IV 1400 Å multiplet were searched for such events, leading to the identification of two explosive events, on 1996 July 10 and 1997 May 31. In both cases, the O IV 1401.16/1404.81 density sensitive line intensity ratio shows a clear variation, corresponding to enhancements in the electron density by factors of  $\sim 3$ . This is fully consistent with recent 2.5D MHD simulations. The 1996 July 10 dataset also provided us with the opportunity to monitor the behaviour of the electron density through an UV blinker. Despite an increase of a factor of two in the line intensities, no variation of the electron density was found. This suggests that the intensity enhancement is due to an increase in the filling factor.

**Keywords:** Sun: Transition region–Ultraviolet: SoHO–Sun: explosive events: electron density:

## 1. Introduction

Brueckner and Bartoe (1983) using observations made with the high resolution telescope and spectrograph (HRTS), described several high velocity events seen in lines from ions formed at transition region temperatures (particularly C IV and Si IV). The authors classified them as turbulent events and jets. The first ones showed velocity components up to  $250 \text{ km s}^{-1}$  with a spatial dimension of  $\sim 2000 \text{ km}$ . Following these first observations, several other authors (Dere, Bartoe, and Brueckner, 1989; Porter and Dere, 1991; Innes *et al.*, 1997a; Chae *et al.*, 1998a; Pérez *et al.*, 1999a; Landi *et al.*, 2000) have studied the phenomena, extending and completing the description of the general characteristics and naming them as ‘explosive events’.

Primarily observed in the network lanes at the boundaries of the super-granulation cells (Porter and Dere, 1991), the explosive events are preferentially found in regions with weak and mixed polarity fluxes that display magnetic neutral lines (Chae *et al.*, 1998a). They are often

---

<sup>†</sup> now at: Osservatorio Astrofisico di Arcetri, 50125 Firenze, Italy



observed in bursts of up to 30 minutes (Innes *et al.*, 1997a; Chae *et al.*, 1998a, Pérez *et al.*, 1999a), while the average lifetime of a single event is  $\sim 60$  s (Dere, 1994). The presence of bi-directional jets (Innes *et al.*, 1997b) with velocities comparable to the local Alfvén speed (Dere, 1994), together with the often observed association with episodes of photospheric magnetic flux cancellation lasting more than 1 hour (Dere *et al.*, 1991; Dere, 1994; Chae *et al.*, 1998a), suggest a sequence of magnetic reconnection events (Parker, 1988; Porter and Dere, 1991; Dere, 1994; Innes *et al.*, 1997b; Wilhelm *et al.*, 1998). Recent MHD modelling of shear-induced magnetic reconnection carried out by Karpen, Antiochos and DeVore (1995) and Karpen *et al.* (1998) shows the appearance of features in which the density is 4-10 times higher than the pre-event local electron density.

A new recently discovered class of transient phenomena characterizing emission lines formed at transition region temperatures was introduced by Harrison (1997) with the name of ‘blinkers’. Observations performed with the CDS spectrometer (Harrison *et al.*, 1995; 1997) on-board SoHO show enhancements in the flux of transition region lines at network junctions (Harrison, 1997; Harrison *et al.*, 1999). Blinkers are mainly observed in lines of O III, O IV and O V with modest or no detectable increase at higher or lower temperatures. They show a typical lifetime of  $\sim 17$  minutes over an area of  $\sim 5 \cdot 10^7$  km<sup>2</sup>, with an average intensity increase in O V of  $\sim 1.5$  which, in extreme cases, can reach values as high as five times the pre-event level (Harrison *et al.*, 1999).

Despite the large number of observational works on UV explosive events and blinkers, large uncertainties about their basic physical parameters such as electron density and temperature still exist. Hayes and Shine (1987), using the ratio of O IV 1401 and Si IV 1402, show some evidence of density enhancements associated with short-lived bursts in an active region. Dere (1994), using the ratio of O IV lines, reports a density of  $7 \cdot 10^{10}$  cm<sup>-3</sup> in an explosive event. More recent indications of density enhancement during explosive events have been presented by Wilhelm *et al.* (1998). In order to derive the electron density of transition region plasma, the most reliable method involves the use of density-sensitive line ratios. However, only lines from the same ion and with similar wavelength should be used (Mason and Monsignori Fossi, 1994; Jordan, 1996; Wikstøl *et al.*, 1998). The fact of belonging to the same ionization stage eliminates the effects of possible differential departure from ionization equilibrium, specially during dynamical events. These constraints are matched by the O IV 1400 Å multiplet (Cook *et al.*, 1995; Brage *et al.*, 1996) which falls inside the wavelength range covered by the SUMER spectrometer on-board SoHO. Wikstøl

Table I. SUMER Quiet Sun observations

Starting Date/Time	Det.	Slit	Exp. Time (s)	Solar X	Solar Y
1996 July 10 17:10	A	1''x120''	20	+ 3	+ 0
1997 May 31 15:01	B	0.3''x120''	12	+600	+576

et al. (1997) presented a critical discussion on many of the possible density sensitive line ratios observable with SUMER, suggesting that the O IV 1400 Å multiplet maybe the only one yielding reliable density diagnostics for the transition region. As shown by Doschek et al. (1998) and O'Shea et al. (2000) lines from O V are also excellent electron density diagnostics. However, for transient events, the O IV lines are more suited due to their count rate. In the present contribution we studied the behaviour of the O IV 1401.16/1404.81 line ratio during the appearance of explosive events and an UV blinker. In the next section we discuss the observations and the data reduction. In § 3, data analysis will be presented, paying particular attention to the problems related to the blends affecting the O IV lines. Results are described in § 4, while their implications and relation to current theoretical models are discussed in § 5.

## 2. Observations and Data Reduction

SUMER is a normal incidence spectrograph operating over the wavelength range  $\sim 500$  to  $1610$  Å (details can be obtained from Wilhelm *et al.*, 1995; 1997; Lemaire *et al.*, 1997). Both of the datasets presented in this work were obtained on the ‘quiet Sun’ in a sit-and-stare mode with no compensation of solar rotation applied.

The 10th July 1996 dataset (see Table I and Figure 1) consists of 42 spectra, exposing for 20 seconds the central part of detector A through a  $1 \times 120$  arcsec<sup>2</sup> slit. For each spectrum, four spectral windows (50 pixels wide) were transmitted to the ground, respectively centered on O IV 1399.77 Å, O IV 1401.16 Å, O IV 1404.81 Å and O IV 1407.38 Å. The selected series of spectra cover a time period of 16 minutes during which, at solar Y= 0, the Sun rotates  $\sim 2.5$  arcsec.

Data for the second dataset were obtained on 31 May 1997 (see Table I and Figure 2) with a  $0.3 \times 120$  arcsec<sup>2</sup> slit on the bottom part of detector B using exposure times of 12 seconds. They consist of a temporal series comprising of 560 spectra. For each spectrum, four spectral

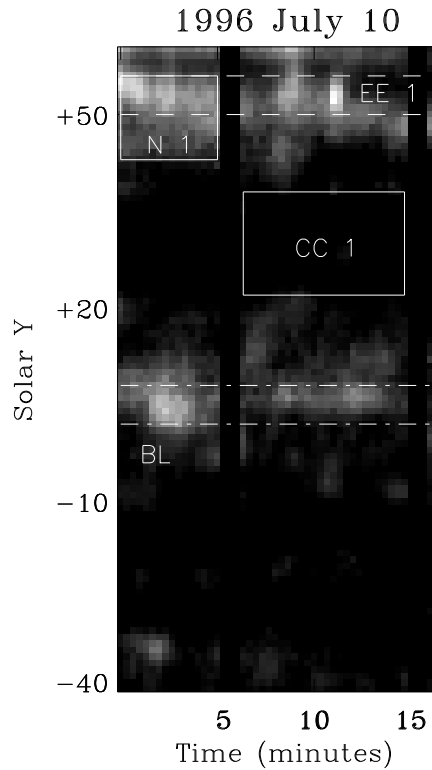


*Figure 1.* O IV 1401.16 intensity map of the 1996 July 10 dataset (DS1). Dashed lines define the region (EE 1) along which the temporal variation of the electron density was followed (see Table II). Areas enclosed by solid lines are the ones over which an integration was performed in order to obtain averaged values for cell center (CC 1) and network (N 1). The evolution of an UV blinker was also studied (BL) along the region defined between the dash-dotted lines. Black columns at 5 and 15 mins. represent missing data.

windows (25 pixels wide) were transmitted to the ground, respectively centered on Si IV 1393.76 Å, O IV 1401.16 Å, Si IV 1402.77 Å and O IV 1404.81 Å. The observations cover a period of 112 minutes, during which the Sun rotates  $\sim 8$  arcsec ( $\sim 27$  times the slit width).

The reduction of SUMER raw images followed several stages, i.e. dead time correction, local gain correction, flat-field subtraction (the July 1996 data were flat-field corrected on-board), radiometric calibration (in order to pass from count  $\text{px}^{-1} \text{s}^{-1}$  to  $\text{Watt m}^{-2} \text{Sr}^{-1} \text{Å}^{-1}$ ) and a correction for geometrical distortion.

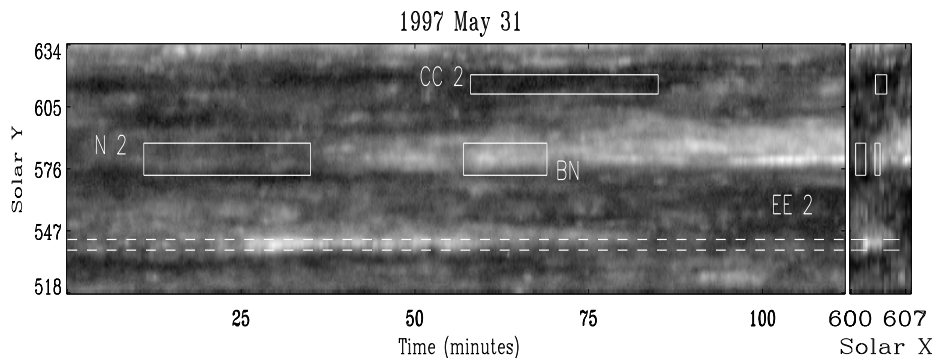


*Figure 2.* O IV 1401.16 logarithmic intensity maps of the 1997 May 31 dataset (DS2). *Left panel:* Time series of the intensity along the slit. Dashed lines define the region (EE 2) along which the variation of the electron density was followed (see Table III). Areas enclosed by solid lines are the ones over which an integration was performed in order to obtain averaged values for cell center (CC 2), network (N 2) and bright network (BN) regions. *Right panel:* The image on the left panel has been binned over groups of 21 slit positions, showing the area of the Sun covered during the entire sequence (see text for details).

### 3. Data analysis

The two datasets studied here present different characteristics which complement each other. The July 1996 dataset (hereafter DS1) contains four O IV lines and offers the possibility to make an evaluation about line blending importance. The large spectral windows allow a precise determination of the line parameters and background contribution. Due to the wider slit it is also possible to achieve a reasonable temporal resolution, while the small drift on the solar surface (2.5 times the slit width) allows us to consider DS1 as an example of the temporal evolution of a ‘quiet Sun’ area at 2 arcsec resolution. The May 1997 dataset (hereafter DS2) presents only two of the oxygen lines belonging to the O IV 1400 Å multiplet. In the DS2 case, the slit covers an area which is 27 times the slit width, resulting more in a raster-type scan than a temporal sequence.

#### 3.1. BACKGROUND SUBTRACTION

In the DS1 case, all line parameters were measured applying a multi-Gaussian fit with a constant background. In the DS2 case, due to the small spectral windows, a different procedure was used. First, a multi-Gaussian fit with constant background was applied in order to measure the background itself and the contribution of S I 1401.51 to the O IV 1401.16 line (see § 3.2). Enhancements in the line wings,

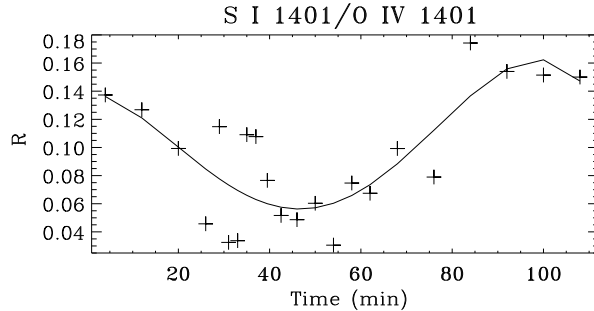


Figure 3. S I 1401.51 to O IV 1401.16 ratio as a function of time/position along EE 2. Crosses represent values obtained from the Gaussian fit, while the solid line represent a spline fit to the data.

particularly during explosive events, can lead to an over-estimation of the background level, particularly for the stronger lines when the small 25 pixel wide spectral window is used. Thus, we decided to use as background values, in all three lines, the ones obtained for the weak O IV 1404.81 line. After this the intensity in the above lines was calculated, integrating over the full spectral window and then subtracting the previously obtained background values. The effect of line blends are, hence, evaluated and removed (see below).

### 3.2. LINE BLENDING

The major problem in measuring transition region electron densities using the O IV 1400 Å multiplet comes from the fact that some of these lines are affected by blending. The situation is even more complex in SUMER data due to the superimposition of second order lines belonging to O III. We only discuss below the O IV lines at 1401.16 Å and 1404.81 Å; problems associated with 1399.77 Å and 1407 Å can be found in Teriaca (2001).

The O IV 1401.16 line ( $^2P_{3/2}^0 - ^4P_{5/2}$ ) is blended with S I 1401.51 Å. This blend can be easily resolved using a two Gaussian fit. The contribution of S I varies from  $\sim 4\%$  of the O IV 1401.16 line in the bright network (BL and BN, see Figures 1 and 2 respectively) up to 37% in the very dark cell center (CC 2, see Figure 2) with average values over the entire datasets of 13% and 12% for DS1 and DS2, respectively. Some difficulties arise during explosive events, when the S I line is blended with the enhanced wings of the O IV line. In the DS1 case, this has been solved using a constrained Gaussian fit where the width and position of S I were obtained from the averaged values over the entire DS1 dataset.

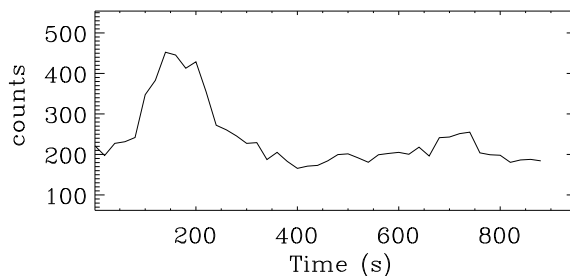


Figure 4. O IV 1401 line intensity variation as a function of time along the central pixel of the BL region showed in Figure 1.

In the DS2 case, the situation was complicated by the small spectral window. Even if any of the explosive events seen in the Si IV lines were visible in the O IV 1401.16 line, it is difficult to estimate the S I contribution as well as the background level. In Figure 3 we can observe the S I/O IV ratio along EE 2. Even if we observe some scatter in the points characterized by the appearance of explosive events, a clear trend from the darker to the brighter regions is clearly visible. From these considerations the final S I 1401.51 contribution to the O IV 1401.16 was obtained applying a spline fit to the data in Figure 3. This assumption is also justified by the observational evidence that explosive events are not observed in lines formed at temperatures below  $4 \cdot 10^4$  K (Dere, 1994).

The O IV line at  $1404.81 \text{ \AA}$  ( $^2P_{3/2}^0 - ^4P_{3/2}$ ) is heavily blended in SUMER data with the O III 702.34 second order line and S IV 1404.771 (Feldman and Doschek, 1979; Cook *et al.*, 1995). These blends cannot be resolved using a line fitting technique and an evaluation using an atomic database is required. The S IV 1404.771 contribution to the total 1404 feature is only 3.6% (Teriaca, 2001).

After correcting for the small contribution of S IV, the CHIANTI (Landi *et al.*, 1999) database was used in order to estimate the theoretical ratio O III (703.845+703.85)/702.34., obtaining a value of 0.2. This compares very well with the measured mean value of 0.212 from SUMER reference spectra for the quiet sun as given by Doschek *et al.* (1999). This line intensity ratio is density independent in the range between  $10^9$  and  $10^{11} \text{ cm}^{-3}$ . The O III 703.845  $\text{\AA}$  and 703.85  $\text{\AA}$  lines are observed as an unique spectral line, hereafter also indicated as O III 703. Using the above value of 0.212 for the ratio O III 703/702.34, the intensity of the O III 702.34 line can be estimated and subtracted from the total intensity of the spectral feature at 1404  $\text{\AA}$ . In DS1, this was done for each chosen area finding that the contribution of O III 702.34 to

the total spectral feature varied between 16% and 37%, with an average value over the entire dataset of 31%. In order to stress the importance of evaluating the O III blend point by point, we also present (see Table II and Figure 7 and 9) the value obtained assuming everywhere a fixed 65% contribution of O IV 1404.81 to the total spectral feature.

In the DS2 case, the 1407 Å spectral feature is not present and the average value of 65% derived above was used for all the selected areas. We conclude that, in average, the blend at 1404 Å comprises ~4% of S IV 1404.771, ~31% of O III 702.34 and, finally, ~65% of O IV 1404.81. Judge *et al.* (1998) for the quiet Sun, suggested an O III contribution of 20% and assumed a zero contribution for S IV. Madjarska *et al.* (1999), studying a prominence, find contributions of 18% and 5% for the two lines respectively.

### 3.3. EXPLOSIVE EVENTS AND BLINKERS IDENTIFICATION

Explosive events are usually observed in strong resonance lines such as C IV 1548 and 1550 or Si IV 1393 and 1402. In DS1, we have only the quite weak O IV intersystem lines around 1400 Å. This makes it difficult to visually identify explosive events. A solution of this problem comes from the closeness between O IV 1401.16 and Si IV 1402.77. The latter is a much stronger line and its left wing is present (weakly) in the right part of the 50 pixel wide O IV window. During an explosive event in which the blue component is present, the amount of Si IV 1402.77 inside the O IV 1401.16 window becomes very large and it appears as a brightening in the O IV 1401.16 intensity map (see Figure 1, along EE 1 at  $t \sim 11$  minutes). In these conditions, only red wing dominated events remain undetected. However, there is evidence for a prevalence of blue wing dominated events over the red wing ones by a factor of 3:2 or more (Dere *et al.*, 1989, Innes *et al.*, 1997a) and in events where both wings are enhanced, the left one is often the strongest (Dere *et al.*, 1989; Landi *et al.*, 2000). Using this technique, an event in DS1 (see Figure 1 and 7) was found at solar Y  $\sim 53$ . The event is clearly present in two successive spectra, leading to a minimum duration of  $\sim 40$  seconds. A region 7 pixels wide (EE 1) was hence selected along the slit (region between dashed lines in Figure 1) and, binning over different time intervals (see Figure 7 and Table II), the line parameters were determined. Further examination shows the explosive event being visible also in the O IV 1401.16 line itself, as an event with a dominant blue-shifted component with a velocity up to  $100 \text{ km s}^{-1}$ . From the position of the left wing of the Si IV 1402.77 line during the event, it is possible to estimate velocities up to  $150 \text{ km s}^{-1}$ .

Another possibility of detecting regions with enhanced dynamical activity is through the analysis of the line width, looking for particularly broad profiles. In fact, transition region and coronal emission lines show a full width half maximum (FWHM) that exceed the Doppler thermal broadening (Mariska, 1992). When opacity effects can be excluded (Doyle *et al.*, 2000), this excess is usually explained through unresolved motion associated with small and large scale motion and/or wave propagation (non-thermal velocity). When we consider all the selected regions in DS1, we note that the FWHM of O IV 1401 is always close to the value obtained averaging over the entire dataset with the exclusion of the region with the explosive event already identified and, partially, with the exclusion of the first region selected along EE 1 (see Table II), where we found a FWHM of 0.327 Å, 30 % larger than the value obtained averaging the entire dataset (instrumental broadening included).

During the first 300 seconds of DS1 it is possible to observe a strong enhancement in the flux of all the spectral features present in the dataset. The brightening is located around solar  $Y = 5$  (see Figure 1) and has an approximate size in the Y direction of  $L \sim 7$  pixels ( $\simeq 5000$  km). In Figure 4, the total intensity in the spectral range around the O IV 1401.16 line (range chosen avoiding the wing of Si IV 1402) is shown as a function of time along the pixel positions passing through the point of maximum brightening (the central pixel of region BL in Figure 1). From Figure 4 it is possible to estimate an approximative duration of  $\sim 200$  seconds for the event under examination. We are not able to determine the dimension in the X direction, but, assuming the same value along the Y direction, we have an area  $\pi L^2 \sim 8 \times 10^7$  km<sup>2</sup>, in agreement with the typical blinker area reported by Harrison *et al.* (1999). A region 7 pixels wide was, hence, selected for DS1 and the temporal evolution of this brightening was followed binning in time over 5 successive spectra (100 seconds) (see Figure 1 and 9).

DS2 was also searched for explosive events performing a visual examination of the Si IV 1393.76 and 1402.77 slit images (see Figure 8), finding a sequence of several explosive events at solar  $Y \sim 540$ , starting approximatively 25 minutes after the beginning of DS2 and lasting  $\sim 30$  minutes. Also in this case a location along the slit was determined (EE 2) and its temporal and spatial evolution studied. In order to have some idea about the presence of enhanced wings due to explosive event activity, we define, for each selected interval along EE 2, the quantity

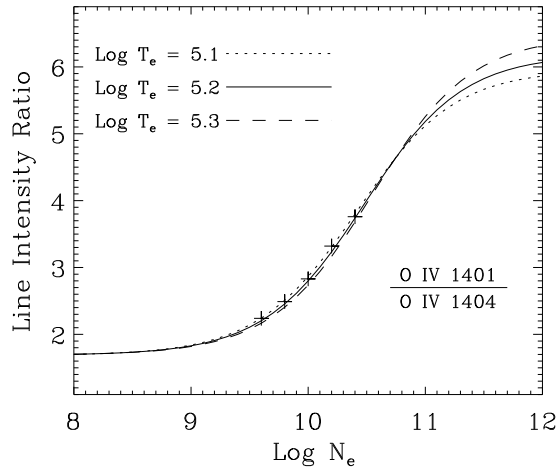


Figure 5. Theoretical dependence of the O IV 1401.16/1404.81 intensity line ratio as calculated with the CHIANTI database for three different temperatures:  $\log T_e = 5.1$  (dotted line),  $\log T_e = 5.2$  (solid line) and  $\log T_e = 5.3$  (dashed line). The crosses represent values of the theoretical line ratio computed by Brage *et al.* (1996) including proton impact excitation at a temperature of  $1.4 \cdot 10^5$  K ( $\log T_e = 5.15$ ).

$W_e$  (wings enhancement) as:

$$W_e = \frac{I_b + I_r}{I_{peak}} \quad (1)$$

where  $I_{peak}$  is the peak intensity of the Si IV 1402.77 Å line, while  $I_b$  and  $I_r$  are the line intensities averaged over 0.17 Å wide intervals centered 0.22 Å away from the central position on the blue and on the red sides of the spectral line. The values of  $W_e$  along EE 2 are reported in Figure 8(b).

### 3.4. LINE RATIOS

The inference of the electron density in an ionized plasma using the line ratio of forbidden lines of transition region ions like O IV has been used by several authors, (eg. Feldman *et al.*, 1976; Dere *et al.*, 1982; Dwivedi and Gupta, 1991; Brage *et al.*, 1996; Wilhelm *et al.*, 1998; Judge *et al.*, 1998; Del Zanna and Bromage, 1999; Pérez *et al.*, 1999b). We use here only the O IV 1401.16/1404.81 intensity line ratio (hereafter  $R_D$ ). Figure 5 shows the variation of  $R_D$  as a function of electron density obtained from the CHIANTI atomic database for three different temperatures:  $\log T_e = 5.1$ , 5.2 (O IV formation temperature) and 5.3. The CHIANTI database allows a complete solution of the

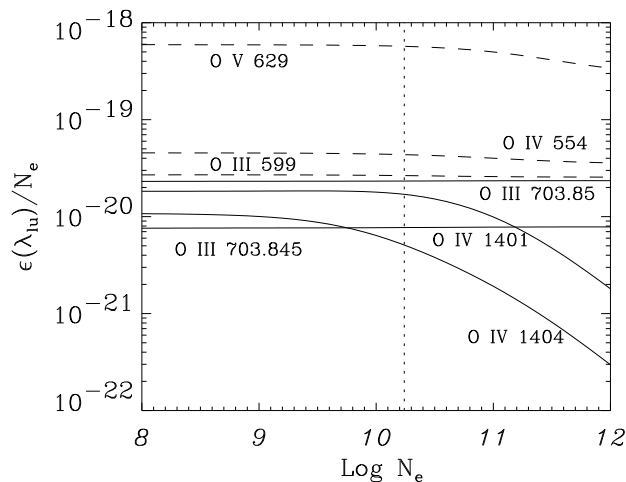


Figure 6.  $\epsilon(\lambda_u)/N_e$  as a function of the electron density as calculated from the CHIANTI database for O III 599, O IV 554, O V 629 (dashed lines) and O III 703.845, O III 703.85, O IV 1401 and O IV 1404 (solid lines). The vertical dashed line represents the maximum density value measured in DS1. For each line, calculations have been performed adopting the formation temperature of the ion to which the line belongs.

statistical balance equation system for the ion in question, including electron impact excitation and de-excitations, but it does not include proton excitation rates. However, proton collisions can be important at redistributing electrons amongst the fine structure levels of a minor species ion formed in the transition region, for example see Doyle *et al.* (1980).

Brage *et al.* (1996) presented theoretical calculations of the  $R_D$  line ratio that include proton excitation. Their results are also shown in Figure 5 and are fully consistent with the ones obtained with CHIANTI. Errors on line intensities determination have been calculated through the photon noise and, hence, the errors on the intensity line ratio established.  $R_D$  shows also a weak temperature dependence resulting in a change of 0.06 for a 0.1 dex variation of  $T_e$  (at  $N_e = 10^{10} \text{ cm}^{-3}$ ). This last error has been quadratically summed to the ones on the intensity line ratio, obtaining the total errors reported in Table II and III. The final errors on the electron density have been evaluated through the CHIANTI database.

One way of verifying whether the observed solar plasma undergoes temperature variation is through the ratio of allowed lines from different ionization stages of the same element (this eliminates uncertainties over abundances). Intensities of lines from allowed transitions respond to

Table II. Results of the 1996 July 10 dataset (DS1). Values in boldface refer to the explosive event.

Time (s)	Ratio <sup>a</sup>	N <sub>e</sub> <sup>a</sup> (cm <sup>-3</sup> )	Ratio <sup>b</sup>	N <sub>e</sub> <sup>b</sup> (cm <sup>-3</sup> )
EE 1				
0 – 79 <sup>(c)</sup>	3.18 ± 0.14	(1.5 <sup>+0.2</sup> <sub>-0.2</sub> ) × 10 <sup>10</sup>	2.94 ± 0.18	(1.2 <sup>+0.2</sup> <sub>-0.2</sub> ) × 10 <sup>10</sup>
80 – 159	2.42 ± 0.11	(6.0 <sup>+1.1</sup> <sub>-1.1</sub> ) × 10 <sup>9</sup>	2.23 ± 0.14	(4.2 <sup>+1.3</sup> <sub>-1.2</sub> ) × 10 <sup>9</sup>
160 – 239	2.79 ± 0.14	(9.9 <sup>+1.7</sup> <sub>-1.6</sub> ) × 10 <sup>9</sup>	2.72 ± 0.19	(9.1 <sup>+2.3</sup> <sub>-2.0</sub> ) × 10 <sup>9</sup>
240 – 319	2.30 ± 0.12	(4.8 <sup>+1.1</sup> <sub>-1.1</sub> ) × 10 <sup>9</sup>	2.11 ± 0.15	(3.2 <sup>+1.3</sup> <sub>-1.2</sub> ) × 10 <sup>9</sup>
420 – 499	2.00 ± 0.12	(2.3 <sup>+1.0</sup> <sub>-1.0</sub> ) × 10 <sup>9</sup>	1.90 ± 0.16	(1.5 <sup>+1.2</sup> <sub>-1.1</sub> ) × 10 <sup>9</sup>
500 – 579	1.77 ± 0.11	(0.6 <sup>+0.8</sup> <sub>-</sub> ) × 10 <sup>9</sup>	1.76 ± 0.14	(0.5 <sup>+0.2</sup> <sub>-</sub> ) × 10 <sup>9</sup>
580 – 659	2.27 ± 0.13	(4.6 <sup>+1.2</sup> <sub>-1.2</sub> ) × 10 <sup>9</sup>	1.98 ± 0.15	(2.2 <sup>+1.2</sup> <sub>-1.2</sub> ) × 10 <sup>9</sup>
<b>660 – 699</b>	<b>3.33 ± 0.23</b>	<b>(1.7<sup>+0.4</sup><sub>-0.3</sub>) × 10<sup>10</sup></b>	<b>2.71 ± 0.23</b>	<b>(0.9<sup>+0.3</sup><sub>-0.2</sub>) × 10<sup>10</sup></b>
700 – 799	2.36 ± 0.14	(5.4 <sup>+1.3</sup> <sub>-1.2</sub> ) × 10 <sup>9</sup>	2.07 ± 0.16	(2.9 <sup>+1.3</sup> <sub>-1.2</sub> ) × 10 <sup>9</sup>
800 – 899	2.01 ± 0.12	(2.4 <sup>+1.0</sup> <sub>-0.9</sub> ) × 10 <sup>9</sup>	1.76 ± 0.13	(0.5 <sup>+0.5</sup> <sub>-</sub> ) × 10 <sup>9</sup>
0 – 899 <sup>(d)</sup>	2.39 ± 0.07	(5.6 <sup>+0.7</sup> <sub>-0.7</sub> ) × 10 <sup>9</sup>	2.16 ± 0.08	(3.6 <sup>+0.7</sup> <sub>-0.6</sub> ) × 10 <sup>9</sup>
BL				
20 – 119	2.43 ± 0.10	(6.1 <sup>+1.0</sup> <sub>-0.9</sub> ) × 10 <sup>9</sup>	2.52 ± 0.14	(6.9 <sup>+1.5</sup> <sub>-1.4</sub> ) × 10 <sup>9</sup>
120 – 219	2.33 ± 0.08	(5.1 <sup>+0.8</sup> <sub>-0.8</sub> ) × 10 <sup>9</sup>	2.45 ± 0.12	(6.3 <sup>+1.2</sup> <sub>-1.1</sub> ) × 10 <sup>9</sup>
220 – 319	2.41 ± 0.10	(5.9 <sup>+1.0</sup> <sub>-0.9</sub> ) × 10 <sup>9</sup>	2.46 ± 0.14	(6.4 <sup>+1.4</sup> <sub>-1.3</sub> ) × 10 <sup>9</sup>
380 – 479	2.35 ± 0.12	(5.3 <sup>+1.1</sup> <sub>-1.1</sub> ) × 10 <sup>9</sup>	2.17 ± 0.14	(3.7 <sup>+1.3</sup> <sub>-1.2</sub> ) × 10 <sup>9</sup>
480 – 579	2.42 ± 0.11	(6.0 <sup>+1.1</sup> <sub>-1.1</sub> ) × 10 <sup>9</sup>	2.40 ± 0.15	(5.8 <sup>+1.5</sup> <sub>-1.4</sub> ) × 10 <sup>9</sup>
580 – 679	2.27 ± 0.11	(4.6 <sup>+1.0</sup> <sub>-0.9</sub> ) × 10 <sup>9</sup>	2.28 ± 0.15	(4.6 <sup>+1.4</sup> <sub>-1.3</sub> ) × 10 <sup>9</sup>
680 – 779	2.33 ± 0.11	(5.1 <sup>+1.0</sup> <sub>-0.9</sub> ) × 10 <sup>9</sup>	2.43 ± 0.16	(6.1 <sup>+1.6</sup> <sub>-1.5</sub> ) × 10 <sup>9</sup>
780 – 879	2.33 ± 0.12	(5.1 <sup>+1.1</sup> <sub>-1.0</sub> ) × 10 <sup>9</sup>	2.44 ± 0.18	(6.1 <sup>+1.8</sup> <sub>-1.6</sub> ) × 10 <sup>9</sup>
ALL 1 <sup>(e)</sup>	2.23 ± 0.06	(4.2 <sup>+0.5</sup> <sub>-0.5</sub> ) × 10 <sup>9</sup>	2.23 ± 0.06	(4.2 <sup>+0.6</sup> <sub>-0.5</sub> ) × 10 <sup>9</sup>
N 1	2.41 ± 0.07	(5.8 <sup>+0.7</sup> <sub>-0.7</sub> ) × 10 <sup>9</sup>	2.26 ± 0.08	(4.5 <sup>+0.7</sup> <sub>-0.7</sub> ) × 10 <sup>9</sup>
CC 1	2.28 ± 0.08	(4.7 <sup>+0.7</sup> <sub>-0.7</sub> ) × 10 <sup>9</sup>	2.30 ± 0.10	(4.8 <sup>+0.9</sup> <sub>-0.9</sub> ) × 10 <sup>9</sup>

<sup>(a)</sup>: Calculated assuming 31% and 3.6% contributions of O III 702.34 and S IV 1404.771, respectively to the total λ 1404 Å spectral feature

<sup>(b)</sup>: Calculated using the local  $R_{1404}^{O\ IV}$  value

<sup>(c)</sup>: Characterized by broad line profile (see text § 3.3)

<sup>(d)</sup>: Average over the entire EE 1 region

<sup>(e)</sup>: Represents the average over the whole dataset

electron density changes in the same way, and any significant change in the line ratio can be read as a signature of a temperature variation.

Following this technique, Harrison *et al.* (1999), using lines such as O III 599, O IV 554 and O V 629 Å, concluded that no significant

temperature variation occurs during blinkers. In our case we have allowed transitions (O III 703.845 and O III 703.85) and an intersystem transition (O IV 1401.16), and we are interested in checking whether the same technique can be used here. In an optically thin plasma the line intensity for a transition from the upper level  $u$  to the lower level  $l$  is given by:

$$I_{lu} = \frac{1}{4\pi} \int_h G(N_e, T_e)_{lu} N_e^2 dh, \quad (2)$$

where  $G(N_e, T_e)_{lu}$  is the *Contribution function* (containing all the density- and temperature-dependent terms). This can be written as:

$$G(N_e, T_e)_{lu} = \frac{\epsilon(\lambda_{lu})}{N_e} \frac{N_{ion}}{N_{el}} \frac{N_{el}}{N_H} \frac{N_H}{N_e}, \quad (3)$$

where  $N_{ion}/N_{el}$  is the relative abundance of the ionic specie obtained from the ionization balance calculations (containing a strong temperature dependence),  $N_{el}/N_H$  is the element abundance with respect to hydrogen and  $N_H/N_e$  the hydrogen abundance relative to the electron density ( $\sim 0.8$ ).  $\epsilon(\lambda_{lu})$  is the emissivity of a spectral line ( $\text{erg cm}^{-3} \text{s}^{-1}$ ) normalized to the number density of the emitting ion  $N_{ion}$  given by:

$$\epsilon(\lambda_{lu}) = \frac{hc}{\lambda_{lu}} \frac{N_u}{N_{ion}} A_{ul}, \quad (4)$$

where  $N_u$  is the population of the upper level  $u$  and  $A_{ul}$  is the spontaneous transition probability from  $u$  to  $l$ . In the case of an isothermal plasma in ionization equilibrium, the ionic fraction can be removed from the integral obtaining:

$$I_{lu} = \frac{1}{4\pi} \frac{N_{ion}}{N_{el}} \frac{N_{el}}{N_H} \frac{N_H}{N_e} \int_h \frac{\epsilon(\lambda_{lu})}{N_e} N_e^2 dh. \quad (5)$$

In Figure 6 we show  $\epsilon(\lambda_{lu})/N_e$  as a function of the electron density for O III 703.845, O III 703.85, O IV 1401 and O IV 1404 (solid lines). The trend for the allowed lines used by Harrison *et al.*(1999) is also shown for comparison (dashed lines). The vertical dotted line indicates the maximum density found in DS1 ( $1.7 \cdot 10^{10} \text{ cm}^{-3}$ ). It is possible to observe how, for densities below this value, the O III 703 and the O IV 1401 lines show the same density dependence (within 3% for  $N_e \leq 10^{10} \text{ cm}^{-3}$  and within 8 % for  $N_e \leq 1.7 \cdot 10^{10} \text{ cm}^{-3}$ ). However, an increase of the electron density (for densities above  $10^{10} \text{ cm}^{-3}$ ) will lead to a reduction of the ratio O IV 1401.16/(O III 703.845 + O III 703.85) (hereafter  $R_T$ ), while an increase in temperature will increase it. Thus,  $R_T$  can be used as an indicator of temperature increases.

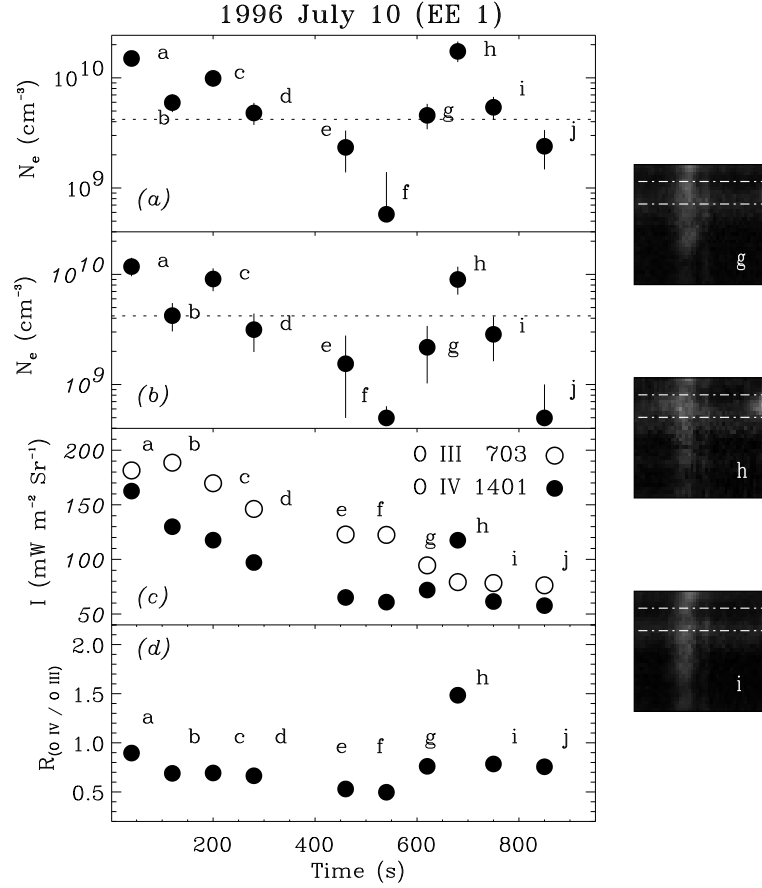


*Figure 7.* Electron density obtained along EE 1. The horizontal dashed line indicates the average density over the whole DS1 (see Table II). (a): Values obtained assuming a fixed 65 % contribution of O IV 1404.81 on the whole 1404 Å feature. (b): Values obtained estimating locally the amount of O IV 1404.81 in the whole 1404 Å feature (see text for details). (c): O III 703 (703.845 + 703.85) (open circles) and O IV 1401.16 (filled circles) line intensities along EE 1 as function of time. (d): O IV 1401.16 to O III 703 line ratio ( $R_T$  within the text) as function of time. *Side panels:* Slit images before (g), during (h) and after (i) the explosive event.

#### 4. Results

Results obtained for DS1 and DS2 are shown in Table II and Figure 7 and 9, and in Table III and Figure 8, respectively. The two datasets considered here have an important difference. As already discussed in § 3, DS1 represents the temporal evolution of a strip of the solar surface ( $1 \times 120 \text{ arcsec}^2$ ) over  $\sim 6$  minutes interval (after which the slit has moved to a new position), while DS2 permits us to build-up a raster

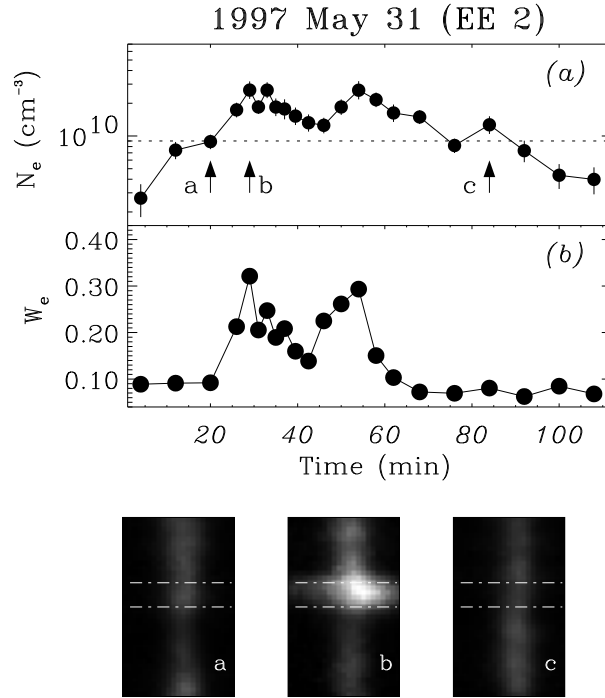


*Figure 8.* (a): Electron density values obtained along EE 2. The horizontal dashed line indicates the average density over the whole dataset (see Table III). These values were obtained assuming a fixed 65 % contribution of O IV 1404.81 on the whole 1404 Å feature. (b): Enhancement factor of the Si IV line wings (see Equation 1). *Lower panels:* Slit images at three specified locations.

of a region  $8 \times 120 \text{ arcsec}^2$  with a resolution of 0.3 and 1 arcsec in the X and Y directions, respectively (see Figure 2, right panel). It is evident that DS2 allows us to identify network and internetwork areas in a more reliable way, while DS1 gives us the possibility of evaluating the importance of the line blends (see § 3.2). The average contribution of O IV 1404.81 to the total 1404 spectral feature (hereafter  $R_{1404}^{O\ IV}$ ) has been evaluated to be 0.65. This value has been adopted for all the measurements in DS2. For DS1 we will discuss the results obtained evaluating locally the  $R_{1404}^{O\ IV}$ , unless specified differently.

#### 4.1. ELECTRON DENSITY IN NETWORK AND INTERNETWORK

Areas of DS1 and DS2 have been selected with the purpose of measuring the electron density in different regions of the solar atmosphere. An average over the whole datasets (ALL 1 and ALL 2) was performed in

order to obtain average density values that can be considered as typical for the quiet Sun.  $N_e$  values of  $(4.2^{+0.6}_{-0.5}) \times 10^9$  and  $(9.0^{+0.7}_{-0.7}) \times 10^9$  cm $^{-3}$  for DS1 and DS2, respectively, were obtained. Electron density values of  $(4.8^{+0.9}_{-0.9}) \times 10^9$  and  $(8.5^{+1.0}_{-1.1}) \times 10^9$  cm $^{-3}$  have been obtained in cell center areas CC 1 and CC 2, respectively, while values of  $(4.5^{+0.7}_{-0.7}) \times 10^9$  and  $(3.9^{+0.6}_{-0.6}) \times 10^9$  cm $^{-3}$  are derived in network areas N 1 and N 2 (see Table II and III). The above results lead to ratios between the electron density in cell centers and network of  $1.1 \pm 0.3$  and  $2.18 \pm 0.3$  for DS1 and DS2, respectively. These values are in agreement with recent results from Del Zanna and Bromage (1999), who report a value of  $1.9 \pm 0.7$ .

It is interesting to note that, in DS1, we obtain a higher value of  $N_e$  in the cell center than in the network, only when the local  $R_{1404}^{O\ IV}$  is calculated. If the  $R_{1404}^{O\ IV}$  values obtained for CC 1 (0.64) and N 1 (0.69) were assumed representative of cell center and network conditions and used to calculate the density in CC 2 and N 2, a still higher ratio between  $N_e$  in cell center and in the network in DS2 ( $3.18 \pm 0.4$ ) could be found. The fact that the  $R_{1404}^{O\ IV}$  is higher in the network than in the cell centers agrees with the fact that the network contrast is higher in O IV than in O III (Gallagher *et al.*, 1998). However, in the region BN of DS2 an electron density of  $(8.7^{+1.0}_{-1.1}) \times 10^9$  cm $^{-3}$  was found, twice the  $N_e$  value found in region N 2 of the same dataset.

#### 4.2. EXPLOSIVE EVENTS: EE 1 AND EE 2

Figure 7 presents the temporal variation of the electron density along EE 1. In Figure 7(a) the electron density, calculated assuming a fixed  $R_{1404}^{O\ IV}$  of 0.65, is shown as a function of time, while in Figure 7(b) values obtained calculating the local values of  $R_{1404}^{O\ IV}$  are reported (see § 3.2). Figure 7(c) shows the intensities of the O IV 1401 (filled circles) and O III 703 (open circles) lines, while the ratio between the intensities of the former and the latter line is showed in Figure 7(d). For reasons of clarity all data points along EE 1 shown in Figure 7 have been identified with a letter from **a** to **j**.

A signature of density variation is evident during the first 300 seconds (**a** – **d**), with a variation of a factor of ( $\sim 2.5$ ) between **a** and **b**. The variation is still large ( $\sim 3$ ) when the local  $R_{1404}^{O\ IV}$  value is used (see Figure 7(b)). During the same time interval the intensity of both lines decreases maintaining a constant ratio  $R_T$  (Figure 7(d)) in all the points except **a**, in which a slight increase is observed. In **a**, an excess in the O IV 1401 line width was detected (see § 3.3). After  $t = 350$  s (see Figure 7) the slit has moved to a different region of the Sun. During the last 400 seconds (**e** – **j**), the intensity of both lines is more or less

constant with the remarkable exception of **h**. This is the point where a strong explosive event was observed (see § 3.3) in the blue wing of the Si IV 1402 line and in O IV 1401.16 Å, with an observed electron density enhancement of a factor  $\sim 3$  with respect to the pre (**g**) and post-event (**i**) values. However, the correction at the time of the explosive event (see Table II, row in bold) is quite problematic due to the difficulties in evaluating the two components of the 1407 blend, in the case that one or both of them could present non-Gaussian components. This would imply a lower limit to the density variation associated with the explosive event. In fact, there is clear evidence that still lower values of density are observed in **f** and **j** (with values  $\sim 7$  and 16 times lower than at the peak of the explosive event, respectively, depending whether a constant  $R_{1404}^{O\ IV}$  value is used or not, see Table II).

In **f** and **j** the intensity of the observed lines is particularly low, leading to large errors in the determination of  $R_D$ . This coupled with the fact that the values falls in the steepest part of the theoretical curve of electron density *versus* intensity line ratio (see Figure 5), leads to large errors in the final electron density. The observed factor of  $\sim 3$  increase in the electron density can, hence, be regarded as a lower limit for the electron density increase. Another reason to consider the above value as a lower limit comes from the dimensions of the integrated area in space and time. In order to have a sufficient S:N ratio, we binned over 40 seconds in time (in point **h**) and over 7 spatial pixels in the Y direction ( $\sim 5000$  km). These values must be compared with an explosive event average life of 60 seconds (Dere, 1994) and typical sizes of 2000 km. The larger integration area, in particular, has probably ‘diluted’ the signature of the explosive event in the quiet Sun background. A sharp increase of  $R_T$ , in correspondence with **h**, is visible in Figure 7(c).

In § 3.4, we have seen how the above line ratio could be used as a probe of the temperature variation in the solar atmosphere, provided the electron density is  $\leq 2.5 \cdot 10^{10} \text{ cm}^{-3}$ . At the density values observed in **h**, the quantity  $\epsilon(\lambda_{lu})/N_e$  for O IV 1401 starts to deviate from a constant value (see Figure 6). In these conditions, an increase in the electron density (at constant temperature) will lead to a reduction in the O IV/O III ratio, so the observed increase in the line ratio cannot be due to the different response of the two lines to an increasing electron density. On the other hand, the value of  $R_T$  in **h** is probably overestimated.

The problem arises in the determination of the O III 703 line intensity, which includes both O III 703.845 and 703.85. In **h**, signatures of the explosive event are observed in Si IV 1402 and in O IV 1401. These two lines have formation temperatures of  $6.4 \cdot 10^4$  and  $1.6 \cdot 10^5$  K, respectively. Since the formation temperature of O III ( $10^5$  K) is just

Table III. Results of the 1997 May 31 dataset (DS2).

Time (min.)	Ratio	$N_e$ ( $\text{cm}^{-3}$ )
1 – 8	$2.05 \pm 0.11$	$(2.7^{+0.9}_{-0.9}) \times 10^9$
9 – 16	$2.57 \pm 0.13$	$(7.4^{+1.4}_{-1.3}) \times 10^9$
17 – 24	$2.70 \pm 0.12$	$(8.9^{+1.4}_{-1.3}) \times 10^9$
25 – 28	$3.33 \pm 0.16$	$(1.7^{+0.3}_{-0.3}) \times 10^{10}$
29 – 30	$3.80 \pm 0.21$	$(2.6^{+0.5}_{-0.4}) \times 10^{10}$
31 – 32	$3.40 \pm 0.15$	$(1.9^{+0.3}_{-0.3}) \times 10^{10}$
33 – 34	$3.80 \pm 0.19$	$(2.6^{+0.5}_{-0.4}) \times 10^{10}$
35 – 36	$3.40 \pm 0.20$	$(1.9^{+0.4}_{-0.3}) \times 10^{10}$
37 – 38	$3.35 \pm 0.23$	$(1.8^{+0.4}_{-0.4}) \times 10^{10}$
39 – 41	$3.20 \pm 0.19$	$(1.5^{+0.3}_{-0.3}) \times 10^{10}$
42 – 44	$3.06 \pm 0.18$	$(1.3^{+0.3}_{-0.2}) \times 10^{10}$
45 – 48	$3.00 \pm 0.16$	$(1.3^{+0.2}_{-0.2}) \times 10^{10}$
49 – 52	$3.40 \pm 0.18$	$(1.9^{+0.3}_{-0.3}) \times 10^{10}$
53 – 56	$3.80 \pm 0.22$	$(2.6^{+0.6}_{-0.5}) \times 10^{10}$
57 – 60	$3.57 \pm 0.17$	$(2.2^{+0.4}_{-0.3}) \times 10^{10}$
61 – 64	$3.26 \pm 0.19$	$(1.6^{+0.3}_{-0.3}) \times 10^{10}$
65 – 72	$3.18 \pm 0.15$	$(1.5^{+0.2}_{-0.2}) \times 10^{10}$
73 – 80	$2.64 \pm 0.11$	$(8.2^{+1.3}_{-1.2}) \times 10^9$
81 – 88	$3.01 \pm 0.18$	$(1.3^{+0.3}_{-0.2}) \times 10^{10}$
89 – 96	$2.56 \pm 0.16$	$(7.3^{+1.7}_{-1.6}) \times 10^9$
97 – 104	$2.25 \pm 0.13$	$(4.4^{+1.2}_{-1.1}) \times 10^9$
105 – 112	$2.20 \pm 0.13$	$(4.0^{+1.2}_{-1.1}) \times 10^9$
1 – 112 <sup>(a)</sup>	$3.04 \pm 0.07$	$(1.3^{+0.1}_{-0.1}) \times 10^{10}$
ALL 2 <sup>(b)</sup>	$2.71 \pm 0.06$	$(9.0^{+0.7}_{-0.7}) \times 10^9$
N 2	$2.19 \pm 0.07$	$(3.9^{+0.6}_{-0.6}) \times 10^9$
CC 2	$2.67 \pm 0.10$	$(8.5^{+1.0}_{-1.1}) \times 10^9$
BN	$2.69 \pm 0.07$	$(8.7^{+1.0}_{-1.1}) \times 10^9$

<sup>(a)</sup>: Averaged over the entire EE 2 region

<sup>(b)</sup>: Represents the average over the whole dataset

in the middle of the previous two temperatures, there is no reason to think that signatures of the explosive event should not be present also in the O III 703 Å line. As discussed in § 3.3, this line (including O III 703.845 and 703.85 observed as one feature) is blended on its blue side

with the 1407.38 O IV line. When a multi-Gaussian fit is performed, the O III line parameters can be easily determined yielding values very close to the ones observed in **g** and **i**. This can be interpreted as the emission coming from background and foreground plasma. In fact, in many explosive events it is possible to identify a rest component with characteristics very close to the ones observed in the surrounding ‘quiet’ plasma (Chae *et al.*, 1998b; Landi *et al.*, 2000). The difficulties come when we look at the O IV line parameters. In this case, we find a very broad profile interpreted as the sum of the O IV background and foreground components plus the enhanced components of O III and O IV. Anyway, even if all the excess (with respect to the value in **g**) of the intensity observed in the broad component is assumed as coming from O III, the value of  $R_T$  in **h** is still higher ( $\sim 30\%$ ) than in **g** and **i**. This suggests that some increase in temperature is occurring during the explosive event. It is worth noting that an increase of  $R_T$  is also observed in **a**, where O IV 1401 shows enhanced broadening that could be interpreted as a small dynamic event. It is important to point out that the same reasoning about the under-estimation of the O III line intensity during the explosive event leads to an over-estimation of the amount of O IV 1404.81 and, hence, again to an under-estimation of the electron density during the explosive event.

In Table III and Figure 8, the results obtained along the region EE 2 are presented. In Figure 8(a), the  $N_e$  values along EE 2 (obtained with a constant  $R_{1404}^{O\ IV}$  of 0.65) are shown, while in Figure 8(b) the wing enhancement quantity  $W_e$  (see Equation 1) is reported. A strong correlation between the electron density and the quantity  $W_e$  appears evident in Figure 8. It is important to remember that, in this dataset, the slit moves to a different area of the Sun after  $\sim 4$  minutes. This means that the values shown in Figure 8(a) and 8(b) may result from both spatial and temporal evolution of the transition region plasma. However, it appears clear that density values  $\sim 3$  times higher than the average over the entire dataset are associated with explosive event-like phenomena. Also in this case the considerations about the size in space and time of the integration area, with respect to the typical values for an explosive event, are valid. Along EE 2 we have an integration in time that, in the best case, is equal to 2 min. and a spatial average over  $\sim 4300$  km. This suggests that the above electron density increase can, once again, be considered as a lower limit.

#### 4.3. THE UV BLINKER

In Figure 9 it is possible to observe the temporal variation of  $N_e$  along the region BL in DS1. In Figure 9(a) the electron density, calculated

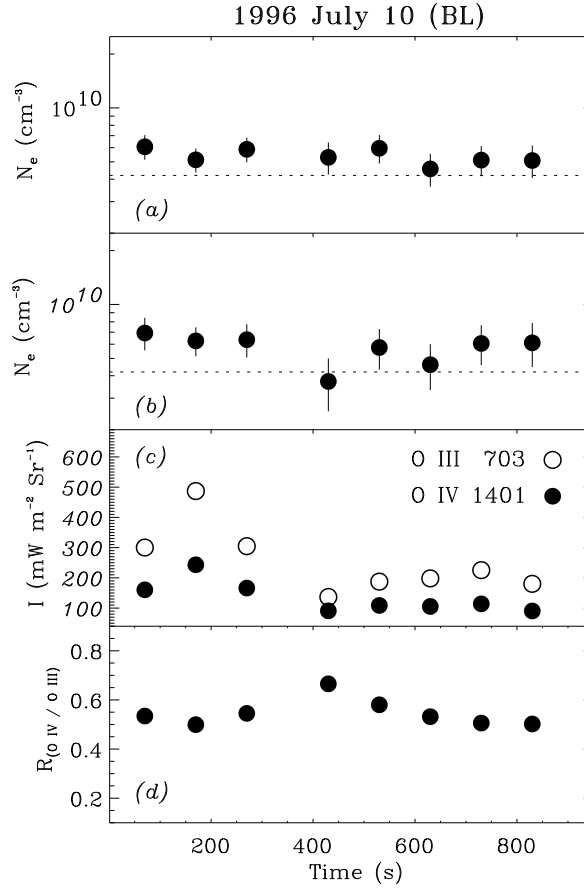


*Figure 9.* Electron density obtained along BL. The horizontal dashed lines indicate the average density over the whole DS1 (see Table II). (a): Values obtained assuming a fixed 65 % contribution of O IV 1404.81 on the whole 1404 Å feature. (b): Values obtained estimating the contribution of O IV 1404.81 on the whole 1404 Å feature through the O III 703 line (see text for details). (c): O III 703 (open circles) and O IV 1401.16 (filled circles) line intensities along BL as a function of time. (d): O IV 1401.16 to O III 703 line ratio ( $R_T$  within the text) as function of time.

assuming a constant  $R_{1404}^{O IV}$  of 0.65, is shown as a function of time, while in Figure 9(b) we report the  $N_e$  values obtained through the local  $R_{1404}^{O IV}$  values (see § 3.2). Figure 9(c) shows the intensities of the O IV 1401 (filled circles) and O III 703 (open circles) lines, while the ratio between the intensities of the former and the latter line is showed in Figure 9(d). It is evident that, when a constant  $R_{1404}^{O IV}$  is used, no appreciable  $N_e$  variation is detected (see Figure 9(a)). The general picture partially changes when the local  $R_{1404}^{O IV}$  value is applied. However, the absence of changes in the electron density during the first

300 seconds remains confirmed, but the situation changes in the second part of the dataset. Starting at  $t = 400$  s,  $N_e$  has reduced by a factor of  $\sim 2$  with respect to previous values. After this point, we observe an increase in  $N_e$  close to the values shown during the first 300 seconds. The  $R_T$  value remains constant for the first three data points (see Figure 9(d)) despite the occurrence of a variation of a factor 1.5 in the line intensities (see Figure 9(c)). The selection of the areas of DS1 over which the binning along BL is performed was done in order to get the region with enhanced intensity inside a single data point (see § 3.3). Nevertheless, the brightening is not uniform across the area defining the second data point. In order to verify whether the electron density is related with the line intensity, a sub-region (two successive spectra times three spatial pixels along solar Y) of the above region was selected around the brightest pixel. Integrating over this sub-region we obtain a higher line intensity (in all lines) but the same electron density as in the second data point.

In Figure 10(a) the spectral profiles around the O IV 1401 line for the first three data points are shown. It is interesting to observe that, for the second data point (dotted line), the O IV 1401 line is broader than for the previous and the following points but without an evident signature of high velocity components like the ones observed during explosive events. The line appears also blue-shifted ( $\sim -5$  km s $^{-1}$ ) compared with the other two data points. When the smaller sub-region centered around the peak of the brightening is considered, the blue-shift increases up to  $\sim -11$  km s $^{-1}$ . During the last 400 seconds a steady decrease of  $R_T$  is observed, while the line intensities do not show any appreciable variation. During the same time period the density appears to increase by a factor of  $\sim 2$ . At electron densities around  $10^{10}$  cm $^{-3}$ ,  $R_T$  should be scarcely affected by the variation in  $N_e$  (see § 3.4). However, the O III 703 line has been used to determine the  $R_{1404}^{O IV}$  (influencing the final determination of  $N_e$ ) as well as the  $R_T$  values (see Figure 9(d)). This can lead, in the case of an under-estimation in the O III line intensity, to an under-estimation of  $N_e$  (through the  $R_{1404}^{O IV}$  value) as well as to an over-estimation of  $R_T$ . We are confident of our measurements of the O III 703 line intensity, but the fact that part of the observed behaviour in the last 400 seconds of Figure 9(b) and 9(d) could be due to the above effect can not be excluded. In any case,  $R_T$  is constant within a factor of 1.2. This is also the level found by Harrison *et al.* (1999) within which the O IV/O III ratio is constant (see Figure 6 in that paper). In Figure 10(b) the spectra around the O IV 1401 line relative to the fourth, fifth, sixth and seventh data points (shown in Figure 9) are reported.

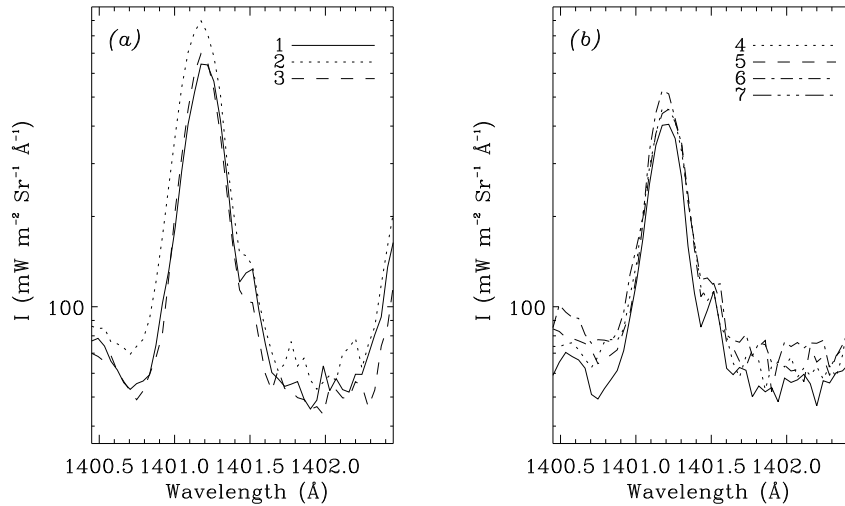


Figure 10. Spectral profiles around the O IV 1401.16 line from BL. Note the blue wing of the Si IV 1402 line partially visible on the right edge of the picture and part of the second order Ar VIII 700.245 on the left edge. The chromospheric S I line at 1401.5136 Å is also clearly visible on the red wing of the stronger O IV 1401 line. In (a) the first three data points of Figure 9 are shown, while in (b) the successive four data point are reported.

## 5. Discussion

In the last decades, the idea of magnetic reconnection as a key process in releasing the magnetic energy, considered the source of numerous solar activity phenomena (from coronal heating to solar flares), has gained importance (Giovanelli, 1946; Gold and Hoyle, 1960; Priest, 1981; Parker, 1988; Forbes, 1991). In the solar atmosphere all the magnetic structures are rooted in the photosphere where the plasma dominates over the magnetic field (plasma  $\beta > 1$ ). In these conditions photospheric motions displace the magnetic structures and opposite polarity fields may, eventually, meet. When this happens the magnetic field may reconnect through the formation of a current sheet, from which plasma is ejected in both directions along the magnetic field lines with velocities of the order of the Alfvén speed. In this context, observations of bi-directional jets with velocities up to  $150 \text{ km s}^{-1}$  (Innes *et al.*, 1997b) together with the detection of associated episodes of photospheric magnetic flux cancellation (Dere *et al.*, 1991; Dere, 1994; Chae *et al.*, 1998a), strongly suggest magnetic reconnection as a possible mechanism for UV explosive events.

Recently, Karpen *et al.* (1995) have performed 2.5 MHD modelling of the interaction between two magnetic dipoles subjected to uniform shearing. Together with the formation of high velocity flows along the current sheet, the authors also report the formation of features with electron densities from 4 to 10 times higher than the pre-event values. Such results have been confirmed in a more recent work by the same authors (Karpen *et al.*, 1998) in which two dipoles of markedly unequal field strength were considered. Also Roussev *et al.* (2000) have recently presented results on the modelling of reconnection jets, again finding electron density increases of a factor of 2–4 in the transition region. In § 4.2 we have shown evidence of enhancements of at least a factor of 3 in the electron density associated with UV explosive events, together with an indication of a possible temperature increase. These observations give further support to the idea that explosive events are signatures of magnetic reconnection occurring in the solar atmosphere.

Another result concerns the evolution of the electron density during an UV blinker (see § 4.3). The blinker studied in the present work shows a duration time of  $\sim 200$  seconds and, hence, can be considered belonging to the short-duration tail of the blinker distribution found by Harrison *et al.* (1999), similarly to the events observed by Gallagher *et al.* (1999). Both of the previous studies were carried out using the CDS spectrometer on-board SoHO. The higher spectral resolution of SUMER permits us to exclude the presence of high velocity motions such as the ones observed during explosive events, at least for the present case (see Figure 10). However, the spectral profile relative to the peak of the blinker (profile 2 in Figure 10a), shows an increased broadening (from an average observed FWHM of  $0.255 \text{ \AA}$  to a value of  $0.285 \text{ \AA}$ ) and a blue-ward shift of  $\sim -5 \text{ km s}^{-1}$ . Chae *et al.* (1998b) suggest that CDS blinkers could consist of several small-scale, short lived SUMER ‘unit brightening events’ with a size of a few arcsec and a lifetime of a few minutes, and characterized by a spectral profile that are not as broad as those of explosive events but still with significantly enhanced wings. They have also suggested that both explosive events and blinkers are due to magnetic reconnection with the differences in the spectral profiles arising from different magnetic geometries.

Harrison *et al.* (1999) proposed a schematic model for UV blinkers, in which newly emerging magnetic flux in cell centers is carried by the convective motions towards the network, where the magnetic field is concentrated (see Figure 13 in that paper). Here the fields merge and, eventually, reconnect through the formation of current sheets. The formation of a current sheet and the resulting formation of shocks and jets should lead to an increase in the electron density (as observed in the case of explosive events), while the thermalization of the accelerated

particles should lead to an increase in the plasma temperature. In the case considered here, no variation in density and temperature is observed, despite an intensity increase of 1.5 – 2 times. This, together with the absence of high velocity motions, strongly suggests that the observed brightening is due to an emission measure increase resulting from the merging of fields carrying plasma at transition region temperatures in the network, as proposed by Harrison *et al.* (1999).

In this context, differences between blinkers and other type of UV transient events could depend on whether magnetic reconnection takes place or not (perhaps also depending on the geometry of the magnetic field). In this view blinkers, Chae's 'unit brightening events' and explosive events could be different examples of progressively higher presence of magnetic reconnection in regions of merging magnetic field.

### Acknowledgements

We would like to thank the anonymous referee for very helpful comments and suggestions. Research at Armagh Observatory is grant-aided by the N. Ireland Dept. of Culture, Arts and Leisure, while partial support for software and hardware is provided by the STARLINK Project which is funded by the UK PPARC. This work was supported by PPARC grant PPA/G/S/1999/00055. The SUMER project is financially supported by DLR, CNES, NASA, and PRODEX.

### References

- Brage, T., Judge, P.G., and Brekke, P.: 1996, *Astrophys. J.* **464**, 1030.  
 Brueckner, G.E. and Bartoe, J.-D.F.: 1983, *Astrophys. J.* **272**, 329.  
 Chae, J., Wang, H., Lee, C.Y., Goode, P.R., and Schühle, U.: 1998a, *Astrophys. J.* **497**, L109.  
 Chae, J., Wang, H., Lee, C.Y., Goode, P.R., and Schühle, U.: 1998b, *Astrophys. J.* **504**, L123.  
 Cook, J.W., Keenan, F.P., Dufton, P.L., Kingston, A.E., Pradhan, A.K., Zhang, H.L., Doyle, J.G., and Hayes, M.A.: 1995, *Astrophys. J.* **444**, 936.  
 Curdt, W., Feldman, U., Laming, J.M., Wilhelm, K., Schühle, U., and Lemaire, P.: 1997, *Astron. Astrophys. Suppl. S.* **126**, 281.  
 Del Zanna, G. and Bromage, B.J.I.: 1999, *J. Geophys. Res.* **104**, 9753.  
 Dere, K.P., Bartoe, J.-D.F., and Brueckner, G.E.: 1982, *Astrophys. J.* **259**, 366.  
 Dere, K.P., Bartoe, J.-D.F., and Brueckner, G.E.: 1989, *Solar Phys.* **123**, 41.  
 Dere, K.P., Bartoe, J.-D., Brueckner, G.E., Ewing, J., and Lund, P.: 1991, *J. Geophys Res.* **96**, 9399.  
 Dere, K.P.: 1994, *Adv. Space Res.* **14**(4), 13.

- Doschek, G.A., Feldman, U., Laming, J.M., Warren, H.P., Schühle, and Wilhelm, K.: 1998, *Astrophys. J.* **507**, 991.
- Doschek, E.E., Laming, J.M., Doschek, G.A., Feldman, U., and Wilhelm, K.: 1999, *Astrophys. J.* **518**, 909.
- Doyle, J.G., Kingston, A.E., and Reid, R.H.: 1980, *Astron. Astrophys.* **90**, 97.
- Doyle, J.G., Teriaca, L., and Banerjee, D.: 2000, *Astron. Astrophys.* **356**, 335.
- Dwivedi, B.N. and Gupta, A.K.: 1991, *Solar Phys.* **138**, 283.
- Feldman, U., Doschek, G.A., and Patterson, N.P.: 1976, *Astrophys. J.* **209**, 270.
- Feldman, U. and Doschek, G.A.: 1979, *Astron. Astrophys.* **79**, 357.
- Forbes, T.G.: 1991, *Geophys. Astrophys. Fluid Dyn.* **62**, 15.
- Gallagher, P.T., Phillips, K.J.H., Harra-Murnion, L.K., and Keenan, F.P.: 1998, *Astron. Astrophys.* **335**, 733.
- Gallagher, P.T., Phillips, K.J.H., Harra-Murnion L.K., Baudin F., and Keenan F.P.: 1999, *Astron. Astrophys.* **348**, 251.
- Giovanelli, R.G.: 1946, *Nature* **158**, 81.
- Gold, T. and Hoyle, F.: 1960, *MNRAS* **120**, 89.
- Hayes, M. and Shine, R.A.: 1987, *Astrophys. J.* **312**, 943.
- Harrison, R.A., Sawyer, E.C., Carter, A.M. *et al.*: 1995, *Solar Phys.* **162**, 233.
- Harrison, R.A.: 1997, *Solar Phys.* **175**, 467.
- Harrison, R.A., Fludra, A., and Pike C.D., *et al.*: 1997, *Solar Phys.* **170**, 123.
- Harrison, R.A., Lang, J., Brooks, D.H., and Innes, D. E.: 1999, *Astron. Astrophys.* **351**, 1115.
- Innes, D.E., Brekke, P., Germerott, D., and Wilhelm, K.: 1997a, *Solar Phys.* **175**, 341.
- Innes, D.E., Inhester, B., Axford, W.I., and Wilhelm, K.: 1997b, *Nature* **386**, 811.
- Jordan, C.: 1996, *Astrophys. J. Suppl. S.* **237**, 13.
- Judge, P.G., Hansteen, V., Wikstøl, Ø., Wilhelm, K., Schühle, U., and Moran, T.: 1998, *Astrophys. J.* **502**, 981.
- Karpen, J.T., Antiochos, S.K., and DeVore, C.R.: 1995, *Astrophys. J.* **450**, 422.
- Karpen, J.T., Antiochos, S.K., DeVore, C.R., and Golub, L.: 1998, *Astrophys. J.* **495**, 491.
- Landi, E., Landini, M., Dere, K.P., Young, P.R., and Mason, H.E.: 1999, *Astron. Astrophys. Suppl. S.* **135**, 339.
- Landi, E., Mason, H.E., Lemaire, P., and Landini, M.: 2000, *Astron. Astrophys.* **357**, 743.
- Lemaire, P., Wilhelm, K., and Curdt, W. *et al.*: 1997, *Solar Phys.* **170**, 105.
- Madjarska, M.S., Vial, J.-C., Bocchialini, K., and Dermendjiev, V.N., 1999, in *Proceedings 8th SoHO workshop*, Paris, ESA SP-446, 467.
- Mariska, J.T.: 1992, *The Solar Transition Region*, Cambridge University Press, Cambridge.
- Mason, H.E., and Monsignori Fossi, B.C.: 1994, *Astron. Astrophys. Rev.* **6**, 123.
- O'Shea, E., O'Neill, T., Keenan, F.P. and Doyle, J.G.: 2000, *Solar Phys.* **196**, 321.
- Parker, E.N.: 1988, *Astrophys. J.* **330**, 474.
- Pérez, M.E., Doyle, J.G., Erdélyi, R., and Sarro, L.M., 1999a, *Astron. Astrophys.* **342**, 279.
- Pérez, M.E., Doyle, J.G., O'Shea, E., and Keenan, F.P.: 1999b, *Astron. Astrophys.* **351**, 1139.
- Porter, J.G. and Dere, K. P.: 1991, *Astrophys. J.* **370**, 775.
- Priest, E.R.: 1981, *Solar Flare Magnetohydrodynamics*, Gordon & Breach, London.
- Roussev, I., Galsgaard, K., Erdélyi, R., and Doyle, J.G.: 2000, *Astron. Astrophys.* (submitted)

- Teriaca, L.: 2001, *PhD thesis* (Queens University/Armagh Observatory).
- Wikstøl, Ø., Judge, P.G., and Hansteen, V.: 1997, *Astrophys. J.* **483**, 972.
- Wikstøl, Ø., Judge, P.G., and Hansteen, V.: 1998, *Astrophys. J.* **501**, 895.
- Wilhelm, K., Curdt, W., Marsch, E., Schühle, U., Lemaire, P., Gabriel, A., Vial, J.-C., Grewing, M., Huber, M.C.E., Jordan, S.D., Poland, A.I., Thomas, R.J., Kühne, M., Timothy, J.G., Hassler, D.M., and Siegmund, O.H.W.: 1995, *Solar Phys.* **162**, 189.
- Wilhelm, K., Lemaire, P., Curdt, W. *et al.*: 1997, *Solar Phys.* **170**, 75.
- Wilhelm, K., Innes, D.E., Curdt, W., Kliem, B., and Brekke, P.: 1998, in *Solar Jets and Coronal Plumes*, Guadalupe, France, ESA-SP 421, 103.